

## **RADAR STUDIES OF AVIATION HAZARDS: Part 3. Frontal Structure Studies**

**Shu-Lin Tung  
F. Ian Harris  
David J. Smalley  
Alan R. Bohne**

**Hughes STX Corporation  
c/o OL-AA PL/GPAB  
29 Randolph Rd.  
Hanscom AFB, MA 01731-3010**

**15 July 1996**

19970206 120

**Scientific Report No. 3**

---

APPROVED FOR PUBLIC RELEASE; DISTRIBUTION UNLIMITED.

---

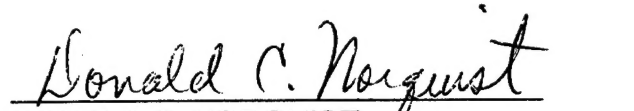



**PHILLIPS LABORATORY  
Directorate of Geophysics  
AIR FORCE MATERIEL COMMAND  
HANSCOM AIR FORCE BASE, MA 01731-3010**

---

"This technical report has been reviewed and is approved for publication."

  
PAUL R. DESROCHERS  
Contract Manager

  
DONALD C. NORQUIST  
Acting Chief, Satellite Analysis and Weather  
Prediction Branch  
Atmospheric Sciences Division

  
DONALD A. CHISHOLM, Acting Director  
Atmospheric Sciences Division

This report has been reviewed by the ESC Public Affairs Office (PA) and is releasable to the National Technical Information Service (NTIS).

Qualified requestors may obtain additional copies from the Defense Technical Information Center (DTIC). All others should apply to the National Technical Information Service (NTIS).

If your address has changed, or if you wish to be removed from the mailing list, or if the addressee is no longer employed by your organization, please notify PL/IM, 29 Randolph Road, Hanscom AFB, MA 01731-3010. This will assist us in maintaining a current mailing list.

Do not return copies of this report unless contractual obligations or notices on a specific document requires that it be returned.

REPORT DOCUMENTATION PAGE			Form Approved OMB No. 0704-0188	
Public reporting burden for this collection of information is estimated to average 1 hour per response, including the time for reviewing instructions, searching existing data sources, gathering and maintaining the data needed, and completing and reviewing the collection of information. Send comments regarding this burden estimate or any other aspect of this collection of information, including suggestions for reducing this burden, to Washington Headquarters Services, Directorate for Information Operations and Reports, 1215 Jefferson Davis Highway, Suite 1204, Arlington, VA 22202-4302, and to the Office of Management and Budget, Paperwork Reduction Project (0704-0188), Washington, DC 20503.				
1. AGENCY USE ONLY (Leave blank)	2. REPORT DATE 15 July 1996	3. REPORT TYPE AND DATES COVERED Scientific No. 3		
4. TITLE AND SUBTITLE  RADAR STUDIES OF AVIATION HAZARDS: Part 3. Frontal Structure Studies		5. FUNDING NUMBERS  F19628-93-C-0054 PE63707F PR 2781 TA GT WU MA		
6. AUTHOR(S)  Shu-Lin Tung, F. Ian Harris, David J. Smalley, and Alan R. Bohne				
7. PERFORMING ORGANIZATION NAME(S) AND ADDRESS(ES)  Hughes STX Corporation c/o OL-AA PL/GPAB 29 Randolph Road Hanscom AFB, MA 01731-3010		8. PERFORMING ORGANIZATION REPORT NUMBER  Hughes STX Scientific Report #10		
9. SPONSORING/MONITORING AGENCY NAME(S) AND ADDRESS(ES)  Phillips Laboratory 29 Randolph Road Hanscom AFB, MA 01731-3010 Contract Manager: Paul R. Desrochers/GPAB		10. PERFORMING ORGANIZATION REPORT NUMBER  PL-TR-96-2178(III)		
11. SUPPLEMENTARY NOTES				
12a. DISTRIBUTION/AVAILABILITY STATEMENT  Approved for public release; distribution unlimited		12b. DISTRIBUTION CODE		
13. ABSTRACT (Maximum 200 words)  Automated techniques have been developed to detect fronts and to extract their three-dimensional structure. Features such as surface frontal position, three-dimensional frontal surface, gradient fields, local wind estimates, and precipitation volume and mass are all monitored as a function of time. These structures and their changes have been related to the development of potentially hazardous weather. Further refinement and testing is required.				
14. SUBJECT TERMS  Doppler weather radar, automated techniques, front detection, front structure, precipitation, front evolution, gradient computation			15. NUMBER OF PAGES 34	
			16. PRICE CODE	
17. SECURITY CLASSIFICATION  Unclassified	18. SECURITY CLASSIFICATION OF THIS PAGE Unclassified	19. SECURITY CLASSIFICATION OF ABSTRACT Unclassified	20. LIMITATION OF ABSTRACT  Unclassified	

# TABLE OF CONTENTS

1	INTRODUCTION .....	1
2	ALGORITHM .....	1
2.1	Overview .....	1
2.2	Methodology .....	3
2.2.1	Preprocessing .....	3
2.2.2	Two-Dimensional Front Detection .....	3
2.2.2.1	Gradient Algorithm .....	4
2.2.2.2	Feature Extraction Procedure .....	5
2.2.2.3	Thin Feature Identification .....	6
2.2.3	Three-Dimension Frontal Structure .....	6
2.2.3.1	Frontal Surface Slope .....	6
2.2.4	Four-Dimension Frontal Evolution .....	7
2.2.4.1	Wind Estimation .....	7
2.2.5	Accessories .....	8
2.2.5.1	Filters .....	8
2.2.5.2	Wind Field Simulation .....	8
3	CASE ANALYSIS .....	8
3.1	Data Description .....	8
3.2	Two-Dimensional Front Detection .....	11
3.2.1	Fine Line Detection .....	11
3.2.2	Gradient Vectors .....	17
3.3	Three Dimensional Structure .....	19
3.3.1	Three-Dimensional Precipitation Boundary .....	19
3.3.2	Frontal Wedge .....	19
4	WIND SHIFT .....	20
5	TIME EVOLUTION .....	24
5.1	General Evolution .....	24
5.1.1	Initial period (2247 05/22/93 - 0142 05/23/93) .....	24
5.1.2	Rapid development period (0142 - 0342) .....	24
5.1.3	Convective dissipation period (0342 - 0523) .....	24
5.2	Front Characteristics .....	26
5.3	Gradient intensity and convective strength .....	28
6	SUMMARY .....	29
7	REFERENCES .....	29

# 1 INTRODUCTION

Baroclinic fronts affect air terminal operations with a variety of weather events, such as abrupt wind shifts, enhanced wind speeds, and accompanying turbulence. Precipitation produced by frontal forcing can be intense and cause flooding. Temperature changes can be abrupt and when combined with precipitation can result in precipitation type changes in non-summer months. For these reasons, the detection and forecasting of fronts is a major concern of weather forecasting services.

Fronts are zones of transition in the temperature and wind fields and their intensity is usually assessed in terms of the magnitudes of the temperature changes and associated wind velocities. Cold fronts, especially, are noted for sharp changes in both temperature and winds. In addition, associated localized intense convection will enhance these fields and may cause severe weather. Fronts always occur in pressure troughs and will always have localized vorticity and convergence maxima. Therefore, monitoring vorticity and divergence in real time could provide useful diagnostic and prognostic information. Single Doppler radar cannot measure these fields individually. However, the radial velocity fields include contributions from these fields and can, therefore, be useful in the detection and monitoring of the fronts and associated phenomena.

In this report, we present a three-dimensional frontal structure algorithm and apply it to a frontal structure analysis. The algorithm employs pattern recognition techniques to manipulate the radar data. Two- and three- dimensional visualization techniques are used to construct the frontal structure and correlate the frontal development with time.

## 2 ALGORITHM

### 2.1 *Overview*

An overall flow chart of the processing procedure for the automatic frontal structure algorithm is shown in Figure 1. The major themes of each unit are:

Pre-processing

- ingest WSR-88D Level II Archive data

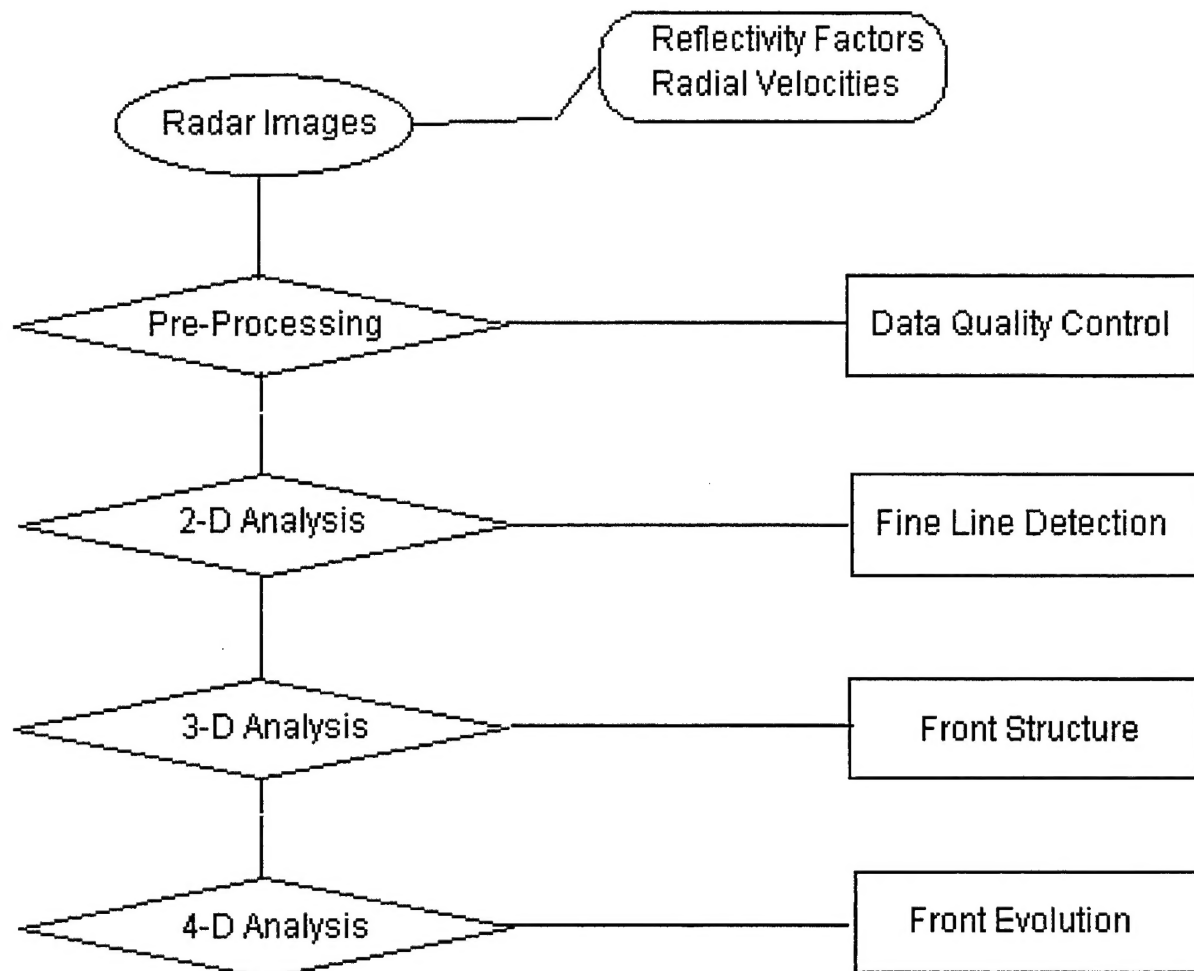


**Figure 1** Processing Procedure of Frontal Structure Algorithm.

- isolate the analysis region
- apply quality control analysis to data

#### Two - Dimensional Frontal Detection

- compute localized gradient vectors of reflectivity factor and radial velocity fields
- apply fuzzy logic to extract frontal region from a combination of data and derived fields
- utilize gradient directions to define frontal line

#### Three - Dimensional Frontal Structure

- construct three-dimensional front boundary from two-dimensional features

- determine frontal slope
- compute sectorized winds
- utilize 3D visualization techniques to analyze airflow and precipitation characteristics
- locate centroid of precipitation area for precipitation distribution

#### Four-Dimensional Frontal Evolution

- analyze frontal properties with time, such as length, orientation, slope, and gradient
- assess frontal propagation
- analyze wind shift
- monitor precipitation development

## **2.2 Methodology**

### **2.2.1 Preprocessing**

As noted above, pre-processing includes the ingestion of the WSR-88D Archive II radar data, the subsectioning of the data to include only the region of interest, and the application of data quality procedures, e.g. thresholding. Most of the routines are standard and will not be highlighted here. The one procedure that is a unique, velocity dealiasing, will be discussed briefly.

A velocity dialiasing procedure based on pattern recognition techniques (Harris *et al.*, 1994; Tung *et al.*, 1995) has been developed to ensure the radial velocity data have been properly dealiasd prior to applying the gradient algorithm. The data are quantized into four equal velocity intervals within the Nyquist velocity range, with each interval being assigned an index corresponding to the velocity interval and a sign corresponding to that of the radial velocity. A map of the data quantized in this manner clearly depicts regions where the data are inconsistent with the surroundings due to aliasing. The data in these regions are then dealiasd.

### 2.2.2 Two-Dimensional Front Detection

Fronts often have distinct convergence lines in the radial velocity field and enhanced lines in the reflectivity factor field (Wilson and Schreiber, 1986). Automated extraction of these features forms the basis of the frontal detection process. There are two basic approaches to the extraction of features within data sets - use of thresholds and the use of gradients. With the use of thresholds, features are extracted by keeping only those regions where the data are within a specific range of values, e.g. above or below a specified value. This is a very simple technique to implement but is highly dependent upon the threshold values that are specified. Gradients are most commonly used for visualization-based techniques, in that our eyes are naturally drawn to regions of enhanced gradients. To numerically extract these regions two-dimensional gradients can be computed and the resultant vector fields can then be analyzed for feature edges, i.e. lines or zones where gradients are maximized. Both of these approaches are used in this development, with the primary emphasis upon the gradient based determinations.

#### 2.2.2.1 Gradient Algorithm

A two-dimensional gradient computation in polar coordinates has been developed (Harris *et al.*, 1994; Tung *et al.*, 1995). The basic technique is an advancement on one developed by Hamann (1991) where several templates were used to determine gradient vectors in Cartesian space. To reduce computations and to increase accuracy, the new method implements a pair of orthogonal finite differencing templates that are defined in polar space. Orthogonal components of the local gradients are determined which then define the gradient vectors.

The local gradient magnitude ( $G$ ) and direction ( $\phi$ ) are computed from difference operators applied in polar coordinates, i.e. along radials at azimuth angle  $\theta$  and arcs at range  $r$  and of length  $s=r\Delta\theta$  :

$$G=(\Delta_r^2+\Delta_s^2)^{0.5}$$

$$\phi=\tan^{-1}(\Delta_s/\Delta_r)$$



$$\text{where } \Delta_r = \frac{\partial f(r,\theta)}{\partial r}, \quad \Delta_s = \frac{\partial f(r,\theta)}{\partial \theta} \frac{\partial \theta}{\partial s}, \text{ and } \frac{\partial \theta}{\partial s} = \frac{1}{r}$$

The gradient vector is aligned along the direction ( $\phi$ ) of maximum change and has a length (G) equal to that maximum change. Gradient vector fields of reflectivity factor and radial velocity are computed for each elevation plane within the volume scan and then used to extract frontal features and to monitor frontal behavior.

#### 2.2.2.2 *Feature Extraction Procedure*

Once the gradients are computed for the reflectivity factor and radial velocity fields, there are six fields that can be used in the front extraction scheme: the reflectivity factor field, radial velocity field, and the gradient magnitude and direction fields for each. Typically, visualization approaches to feature extraction involve the detection of edges denoting perimeters or lines within those features. These edges are defined as lines or zones where there are very large gradients. In the reflectivity factor field, because the largest gradients tend to be on the boundaries of echoes, edges based on gradients can usually define the perimeter of a radar echo. In radial velocity fields, large gradients tend to occur across the wind shift lines associated with the front. The regions with large gradient magnitudes and somewhat coherent vector directions are isolated for both reflectivity factors and radial velocities. This sometimes results in multiple regions, some of which have no relationship to the front in question. To eliminate small, insignificant regions, an image thresholding technique is applied to extract the major interest edges associated with fronts. Fuzzy logic is used to combine interest edges into a coherent frontal region. For cold fronts, the reflectivity factor fields are given the greatest weighing while for gust fronts radial velocity gradient fields receive the most attention.

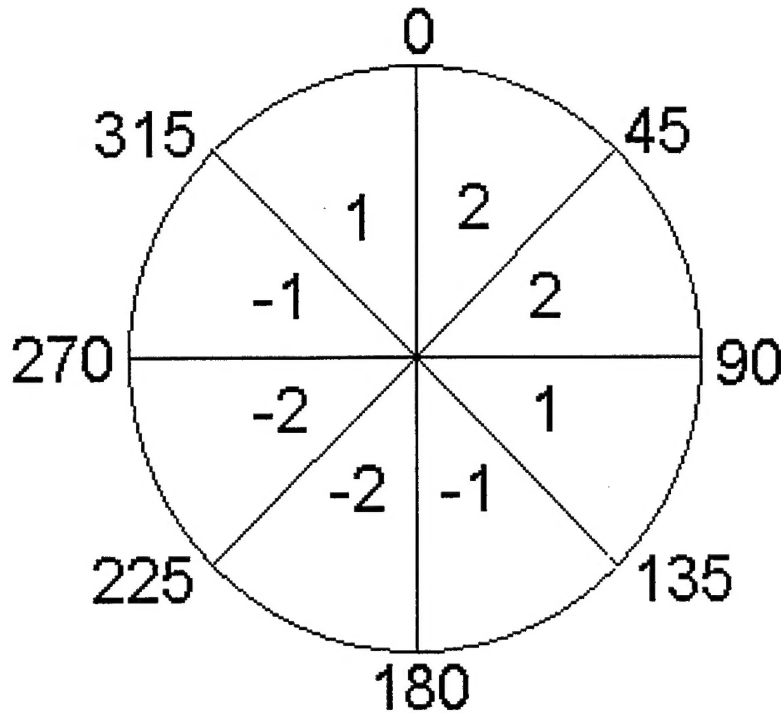


**Figure 2** Octant Indices.

### 2.2.2.3 *Thin Feature Identification*

The feature extraction procedure produces a broad frontal zone region.

However, in practice, a more focused feature is desired. A technique that utilizes gradient vector directions is used to reduce the broad line to a thin line. Octant values are derived based on the configuration shown in Figure

2. An octant value is determined by the direction of the gradient vector relative to a reference angle (e.g., the 90° axis or mean front orientation). This results in well-defined positive and negative regions with a sharp transition line oriented along the detected front. This line is then easily extracted for monitoring purposes.

## 2.2.3 Three-Dimension Frontal Structure

### 2.2.3.1 *Frontal Surface Slope*

An algorithm has been developed to compute the slope of the cold front surface, the leading surface of the wedge of cold air. Typically, the winds in the warm air ahead and above the cold front are from a direction that is at least 90° from that of the cold air. This means that there is often significant wind shear in the transition zone between the cold and warm air. In Doppler radar data, this transition will usually result in distinct vertical shear of the radial velocities, especially when the radar beam is approximately orthogonal to the front. When the front is approaching the radar, this surface can be generated by identifying the top

of the domain where the radial velocities have a component directed towards the radar. Then, the slope at each point on this surface is computed with the two-dimensional gradient algorithm applied to the height field associated with this surface. Complications are introduced to this computation scheme through the presence of spurious or missing data and when the front has passed by the radar. Missing and spurious data produce gradients opposite in direction from those due to legitimate data and are therefore readily identifiable. The problems introduced when the front has passed the radar are more complex and remain to be mitigated.

## 2.2.4 Four-Dimension Frontal Evolution

### 2.2.4.1 Wind Estimation

An algorithm adapted from Hermes *et al.* (1993) has been developed to estimate the winds near the front. This technique assumes the wind field to be uniform and horizontal within a specified sector. The mean horizontal wind  $(u_0, v_0)$  and the radial velocities in the sector are related as follows:

$$\sum_i V_{ri} = u_0 \sum_i \sin \theta_i + v_0 \sum_i \cos \theta_i$$

Through a least squares technique, an estimate of the mean wind within a sector can be obtained, where  $\theta_i$  is the azimuth angle measured clockwise from north. Solutions are sensitive to the distribution of the actual winds in the sector and the angular dimension of the sector. They are relatively insensitive to the range domain of the sector. It is important that the sector be large enough to allow adequate resolution but small enough so that the uniform wind assumption within the sector is valid. It has been found that a sector size of 80° azimuthal extent and 30 km range extent should be sufficient for good uniform wind estimation.

## **2.2.5 Accessories**

### **2.2.5.1 *Filters***

Several kinds of filters are used throughout the analysis procedures. They include:

- A uniform filter designed to average data over a variable-sized box.
- A filter designed to retain only data that have sufficient surrounding data where both the size of the filter and the minimum number of surrounding data points are user specified. This has been used to eliminate noise.
- A filter provided by AVS ( a visualization software package) to compute localized minima, maxima, medians, and means within data fields.

### **2.2.5.2 *Wind Field Simulation***

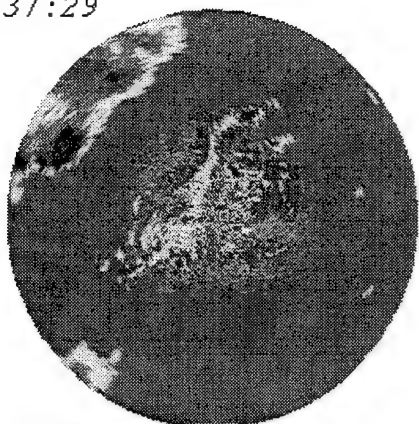
A simple model has been developed to simulate kinematic motions. The simulation is controlled through widgets. Any kind of simple motion structure can be easily simulated and placed on the desired location. In general, the motion about a point can be described in terms of local means and derivatives. In meteorological or fluid dynamical terms, this means wind speed and direction, divergence, vorticity, and deformation. This module allows the user to specify location and magnitude parameters for each of these fields. It then uses these parameters to generate data with fields consistent with these specifications. This model has been used in algorithm development to generate simulation fields for testing.

## **3 CASE ANALYSIS**

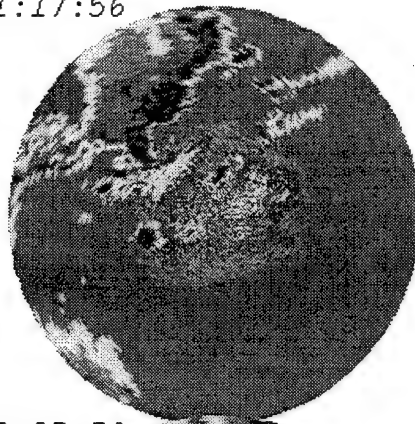
### **3.1 *Data Description***

A front was observed over an extended period by the WSR-88D Doppler radar at Dodge City, KS, during May 22-23, 1993. Figure 3a depicts the reflectivity factor field at

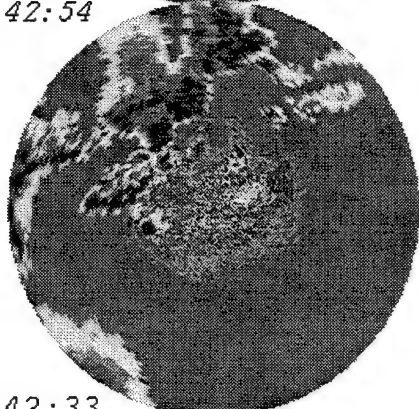
23:37:29



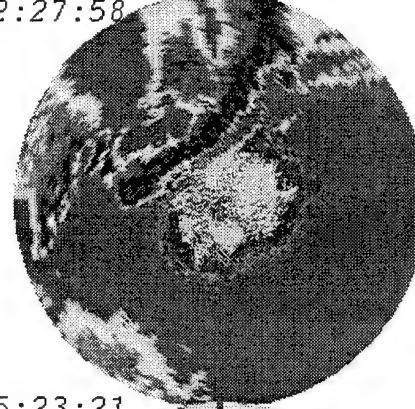
01:17:56



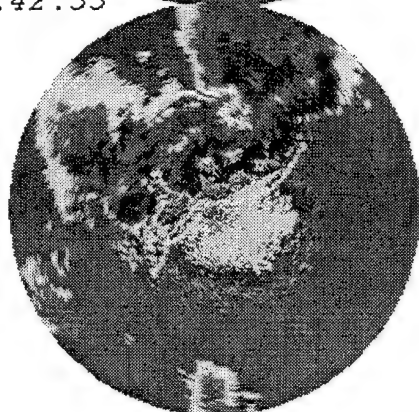
01:42:54



02:27:58



03:42:33



05:23:21

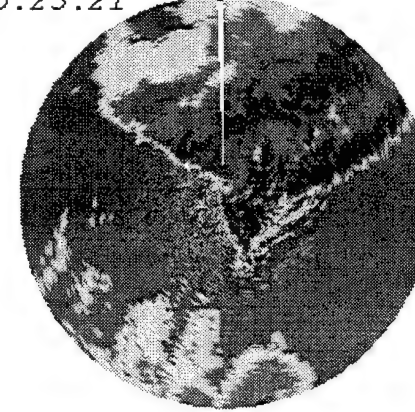


**Figure 3a** Reflectivity factor fields at 0.5° elevation.

23:37:29

01:17:56

01:42:54

02:27:58

03:42:33

05:23:21

-64 -43 -22 0 22 43 64

**Figure 3b** Radial velocity fields at 0.5° elevation.

0.5° elevation for selected times during the observational period. The maximum range for these displays is 230 km. In this figure, a northeast to southwest line of convection associated with the cold front moves from northwest to southeast during the observational period, passing the Dodge City WSR-88D radar about 0345 UTC on 05/23/93. A thin line in the warm sector ahead of the front moved from near the radar at 2337 UTC on 05/22/93 toward the northwest (i.e. towards the front) and merged with the pre-frontal gust front around 0142 on 05/23/93. By 0227 the enhanced convective development that occurred along the cold front after the merger of the cold front and the thin line can be seen. After this time, the convection dissipates as the pre-frontal line moves away from the cold front.

Figure 3b depicts radial velocity corresponding to the reflectivity factors displays in Figure 3a. The flow behind the cold front is from the west to northwest, roughly orthogonal to the cold front itself. The local environmental winds ahead of cold front are from south to southwest. Before 0117, there is strong convergence along the leading precipitation edge. Then, the strong convergence moves ahead of the precipitation by 0227 and is more associated with a gust front that has developed.

From both the reflectivity factor and Doppler velocity fields, this front appears to be the best developed within this sequence at 0227. This particular volume is used for the following analysis presentations.

## **3.2 Two-Dimensional Front Detection**

### **3.2.1 Fine Line Detection**

Figures 4a-f depict products at various stages of the fine line detection for the volume scan at 0227. The methodology for detection is based on the pattern recognition techniques discussed in Section 2. Figures 4a and 4c depict the reflectivity factors and radial velocities, respectively, at the lowest elevation (0.5°) while Figures 4b and 4d depict the corresponding gradient fields. In these figures, a long cold front is observed, especially in the reflectivity factor and reflectivity factor gradient fields (Figures 4a and b), along with a short gust front (Figure 4d) to the southeast of the cold front. The procedure for extraction of these lines

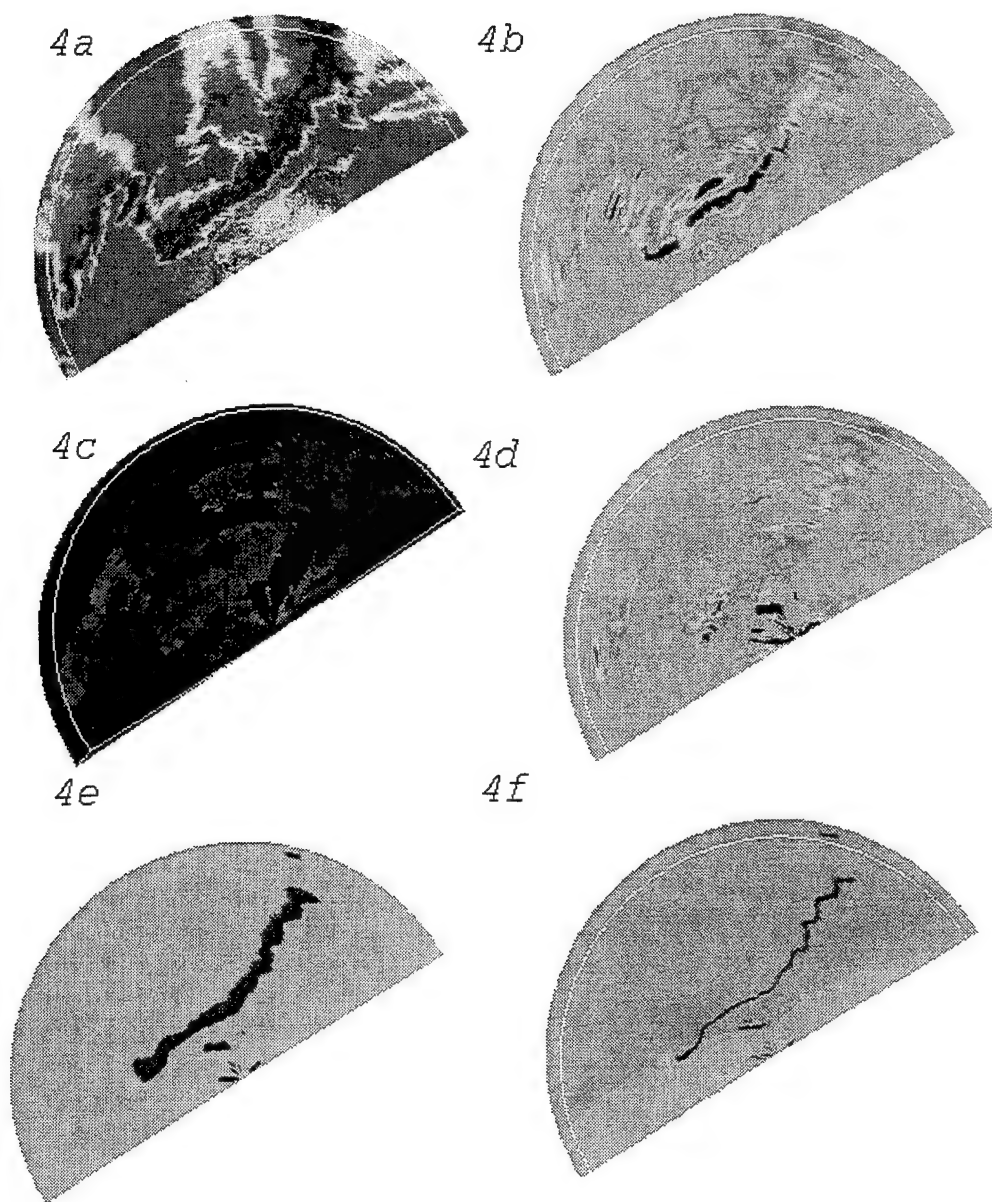


**Figure 4a-f** 2D Fine Line Detection.



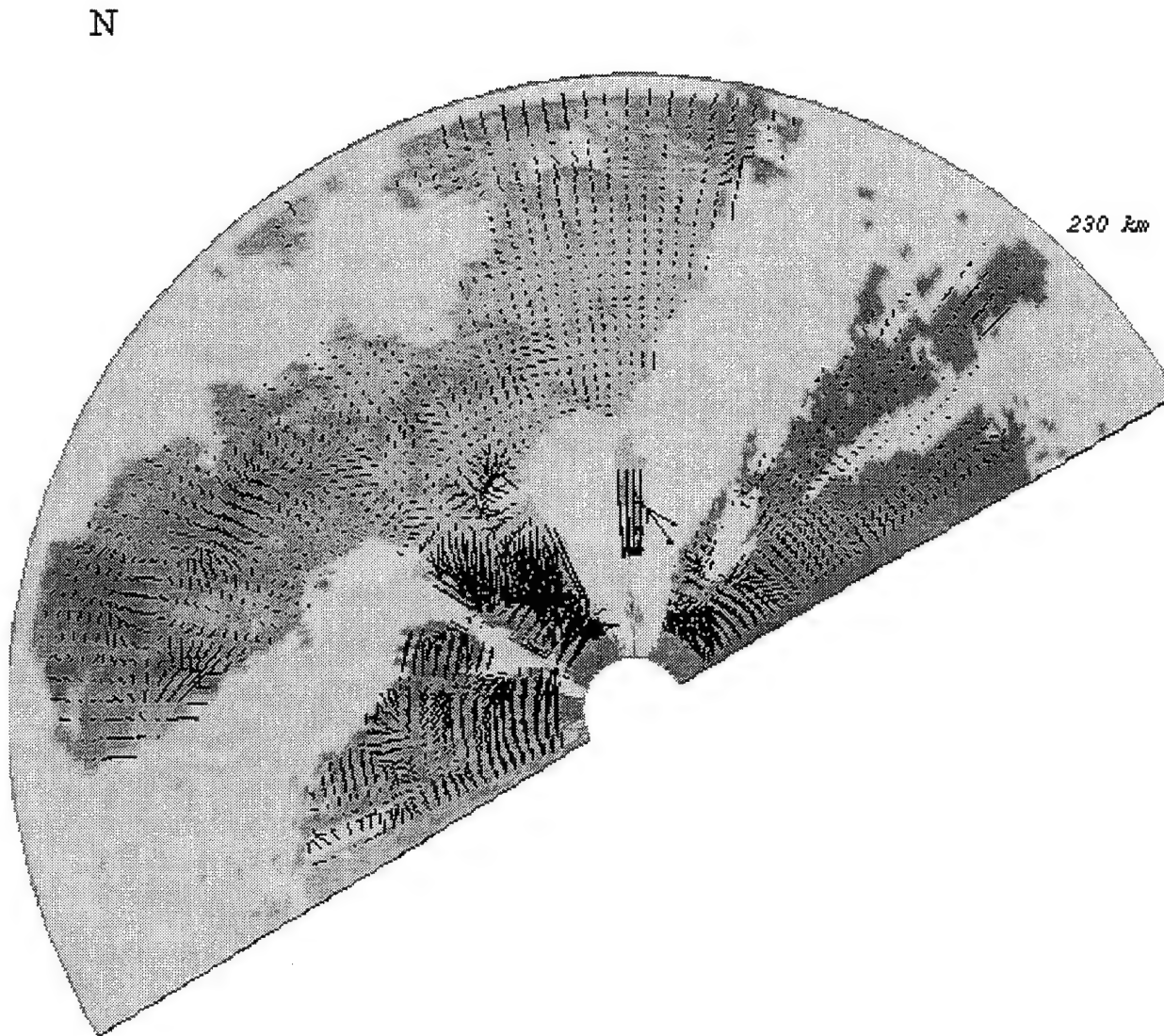


**Figure 5a** Radial velocity gradient vectors superimposed with radial velocity field at elevation  $0.5^\circ$ .

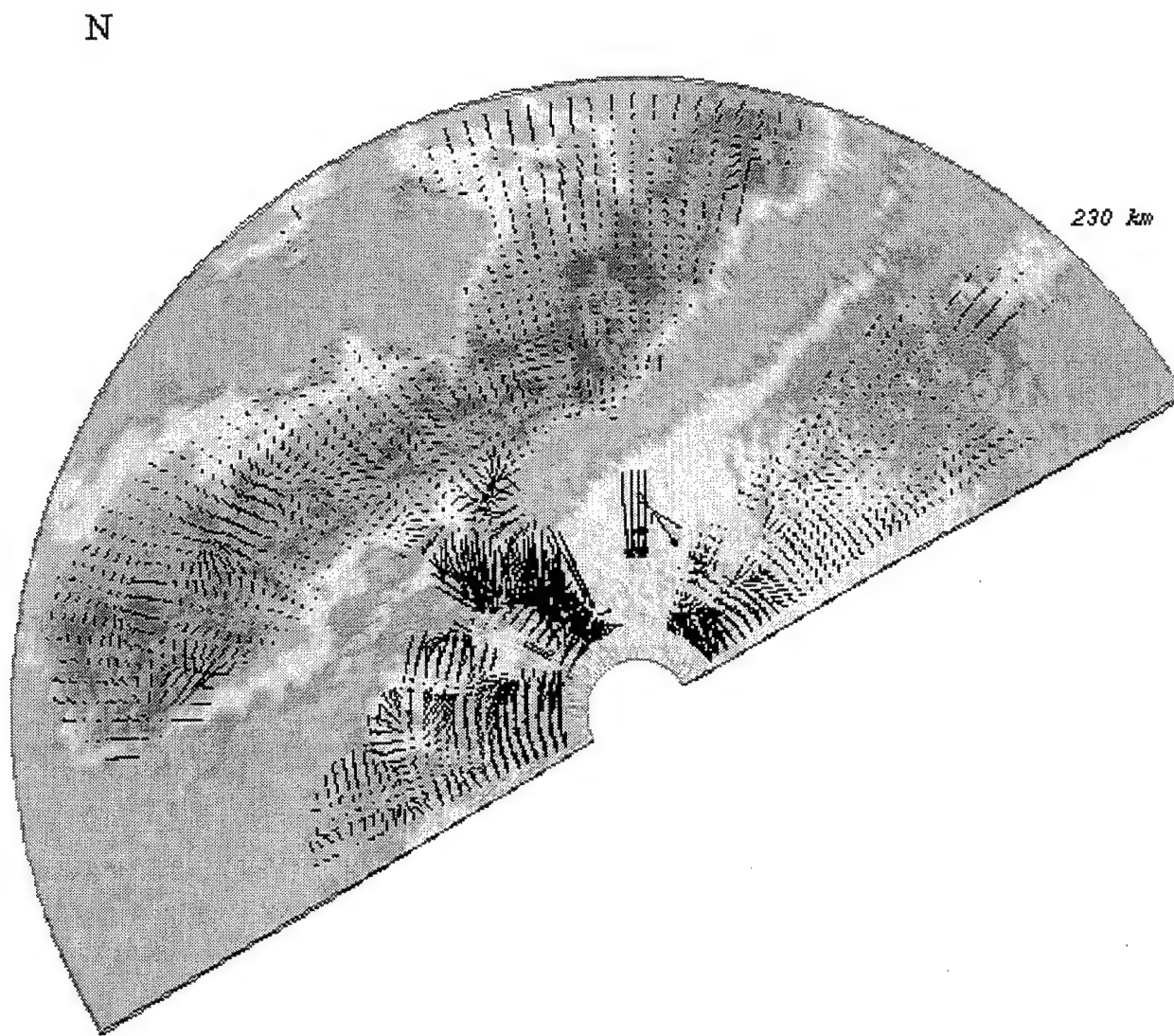


**Figure 5b** Radial velocity gradient vectors superimposed with reflectivity factor field at elevation  $0.5^\circ$ .

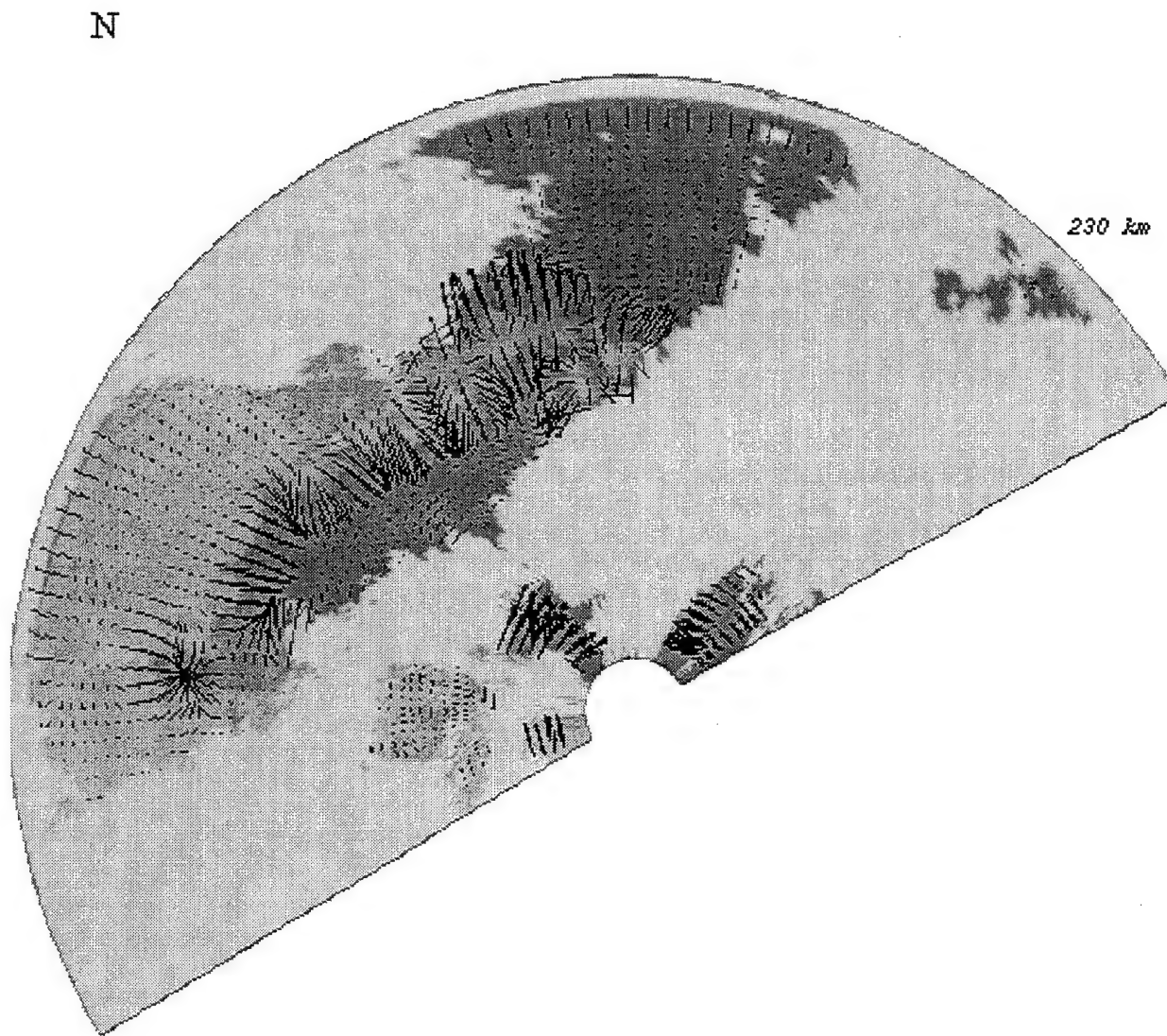


**Figure 6a** Radial velocity gradient vectors superimposed with radial velocity field at elevation  $2.4^\circ$ .

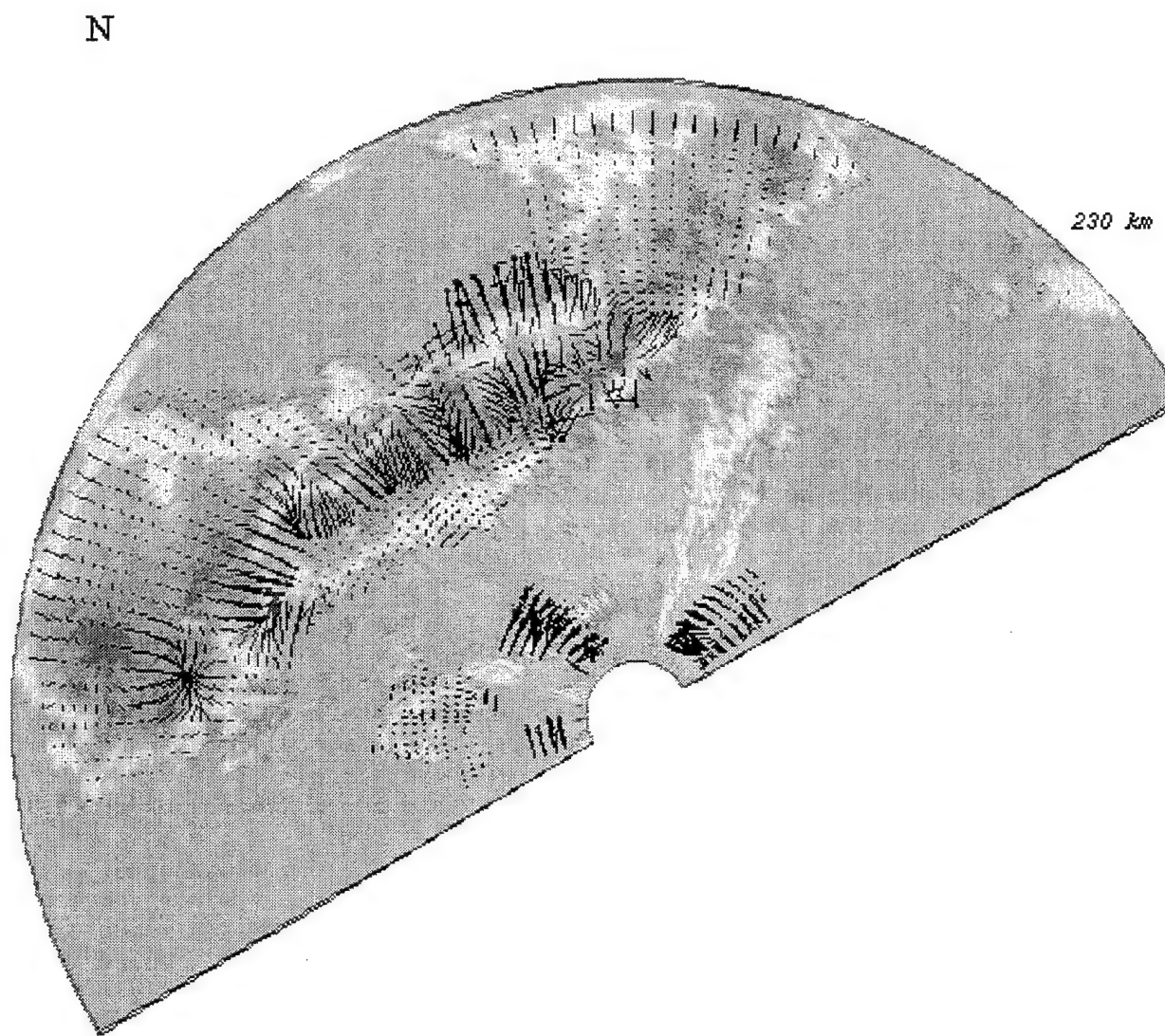


**Figure 6b** Radial velocity gradient vectors superimposed with reflectivity factor field at elevation  $2.4^\circ$ .

focuses on the reflectivity factor and reflectivity factor gradient fields for the cold front and on the velocity gradients for the gust front. Gradient thresholds were used to extract edges of the reflectivity factor areas and strong shear zones in the radial velocity fields. The domains from each of these analyses are combined using fuzzy logic (Figure 4e) where the resultant domains and the reflectivity factor gradient directions are plotted. The gradient directions are converted to relative angles with respect to east and indices are assigned according to directional octant (see Figure 2). The positive (negative) region contains the gradients from low to high (high to low). This quantization of the data results in a distinct line between the positive and negative gradients that lies along the assumed frontal position. The gradient edge detection is applied again on either positive region or negative region to detect the outline edges. The line between the positive region and the negative region can be extracted as a frontal fine line (Figure 4f).

### 3.2.2 Gradient Vectors

The gradient vectors for the radial velocities are shown in Figures 5 and 6 at elevations of  $0.5^{\circ}$  and  $2.4^{\circ}$ , respectively. Figures 5a and 6a show the vectors superimposed on the radial velocity fields while Figures 5b and 6b have the vectors on the reflectivity factor fields. The strongest convergence (longest gradient vectors directed towards the radar) occurs near the pre-frontal wind shift line at  $0.5^{\circ}$ . This is well ahead of the maximum reflectivity factor line. At  $2.4^{\circ}$  (Figure 6), the strongest convergence occurs on the maximum reflectivity factor line associated with the cold front surface. This suggests that the low level forcing by the gust front is insufficient to overcome any stability that there may be in the very lowest levels of the warm air ahead of the front. However, there appears to be sufficient lifting at the cold front itself to overcome this stability and result in the observed deep convection along the front. These observations are from the evening hours, a time when radiation cooling tends to stabilize the boundary layer of the atmosphere.

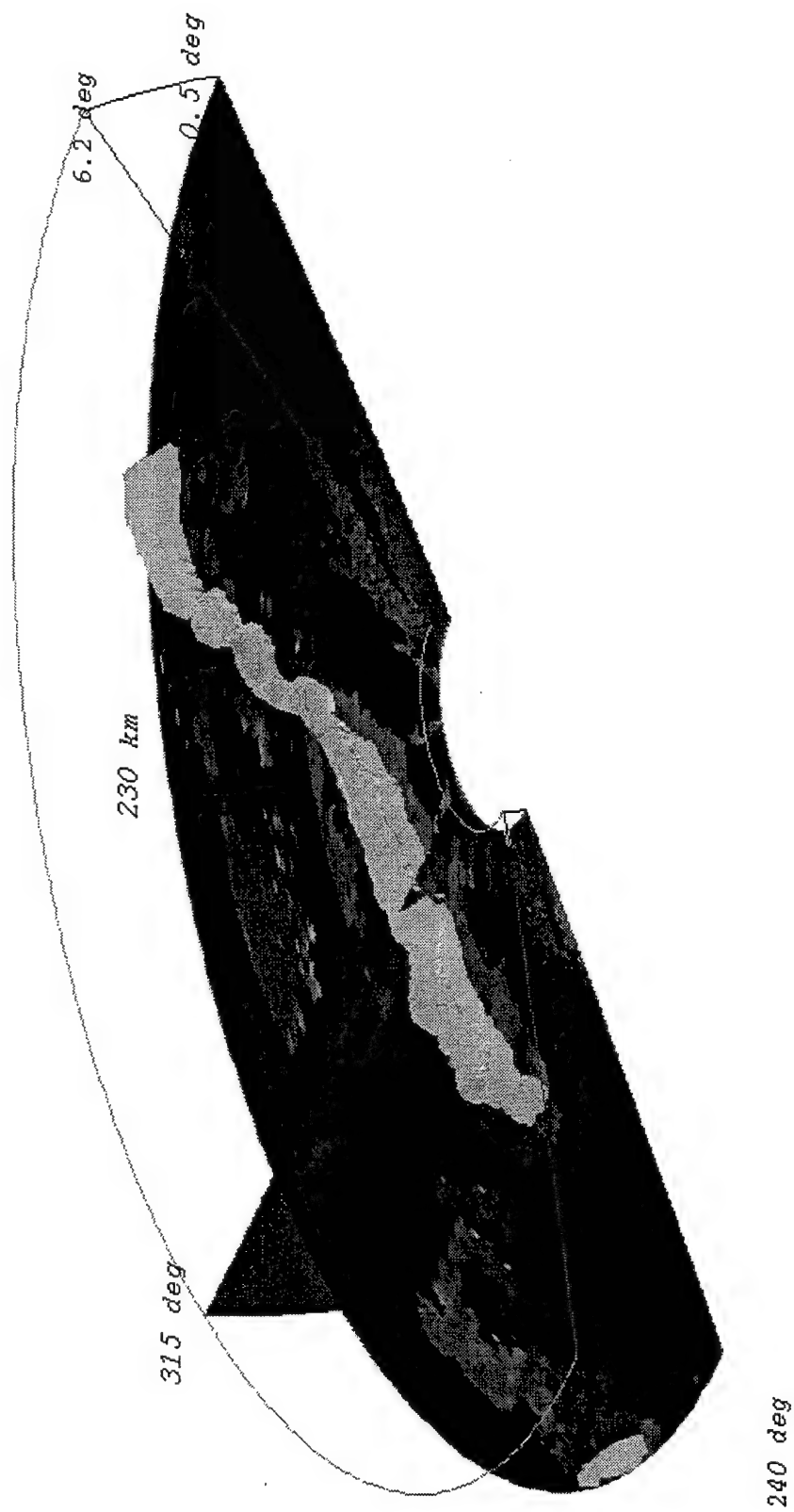


**Figure 7** Detected 3D Frontal Precipitation Boundary.

### 3.3 Three Dimensional Structure

#### 3.3.1 Three-Dimensional Precipitation Boundary

The two-dimensional regions detected at each elevation are combined to build a three-dimensional boundary which is really a boundary for the more intense precipitation along the front (Figure 7). While this boundary is not the true frontal boundary at higher elevations, it is significant in terms of location of hazardous weather.

#### 3.3.2 Frontal Wedge

In the lower atmosphere to the northwest of the front, the air has velocity components towards the radar, i.e., from the northwest. Since the front has not passed the radar, a volumetric display of only negative (components toward the radar) velocities results in a wedge that slopes upward toward the northwest (Figure 8). The two vertical sections through

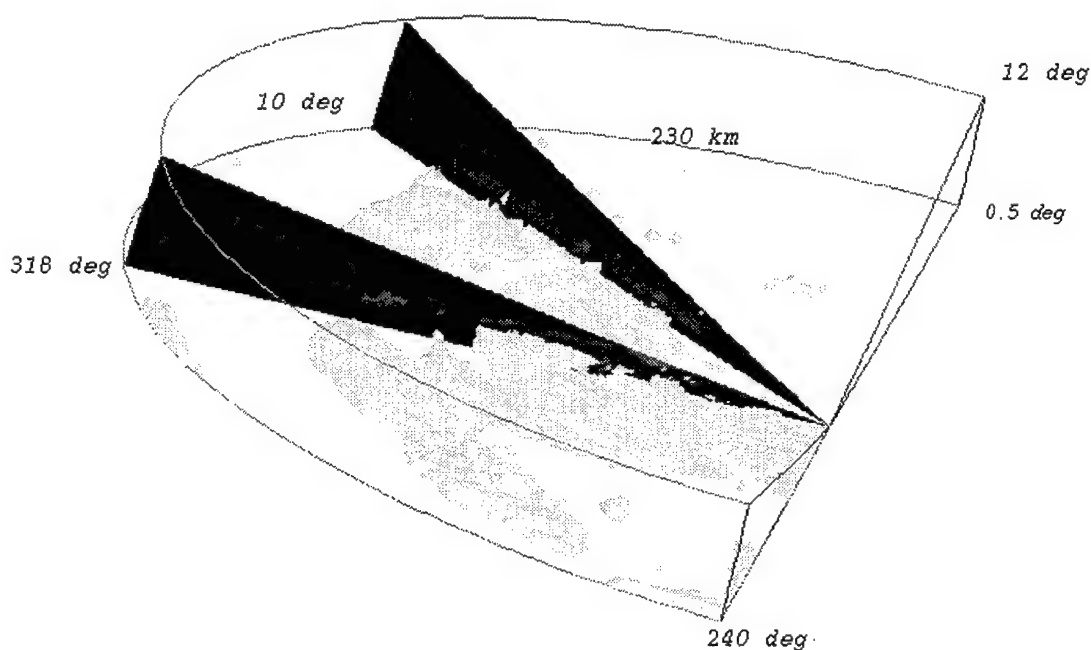


**Figure 8** Cold Front Wedge.



this wedge show that, above the northerly cold air flow, there are positive velocities, indicating the southerly components in the warm air above and ahead of the front. The upper surface of this wedge appears to be a reasonable representation of the frontal surface.

The vertical coordinates of wedge top represent the height field of the frontal surface in Figure 8. The gradients of this height field are computed which represent the slope field for the frontal surface. Negative gradients and extremely high values have been eliminated resulting in a relatively smooth, positive gradient field. The overall frontal surface slope is approximated by the median of the slope field and found to be about 0.02~0.03, which corresponds to a vertical to horizontal ratio of  $1/50 \sim 1/30$ , reasonable values for a cold front.

## **4 WIND SHIFT**

The uniform wind sector method is applied to generate the estimates of the winds ahead and behind the front for wind shift analysis. Figures 9 a-c depict the wind vectors for the lowest radar scans estimated by the uniform wind sector method along with the detected cold and gust fronts at 0142, 0227, and 0247, respectively. It is to be noted that the vectors emanate from their respective data location points. Throughout these three displays we see that the velocities behind and immediately ahead of the cold front have northerly components. The only strong southerly component vectors occur south of the gust front. In addition, the strongest cross front components are seen on the east side of these data. Before these estimates can be used with appreciable confidence, they need to be verified through comparisons with independent data such as surface measurements.



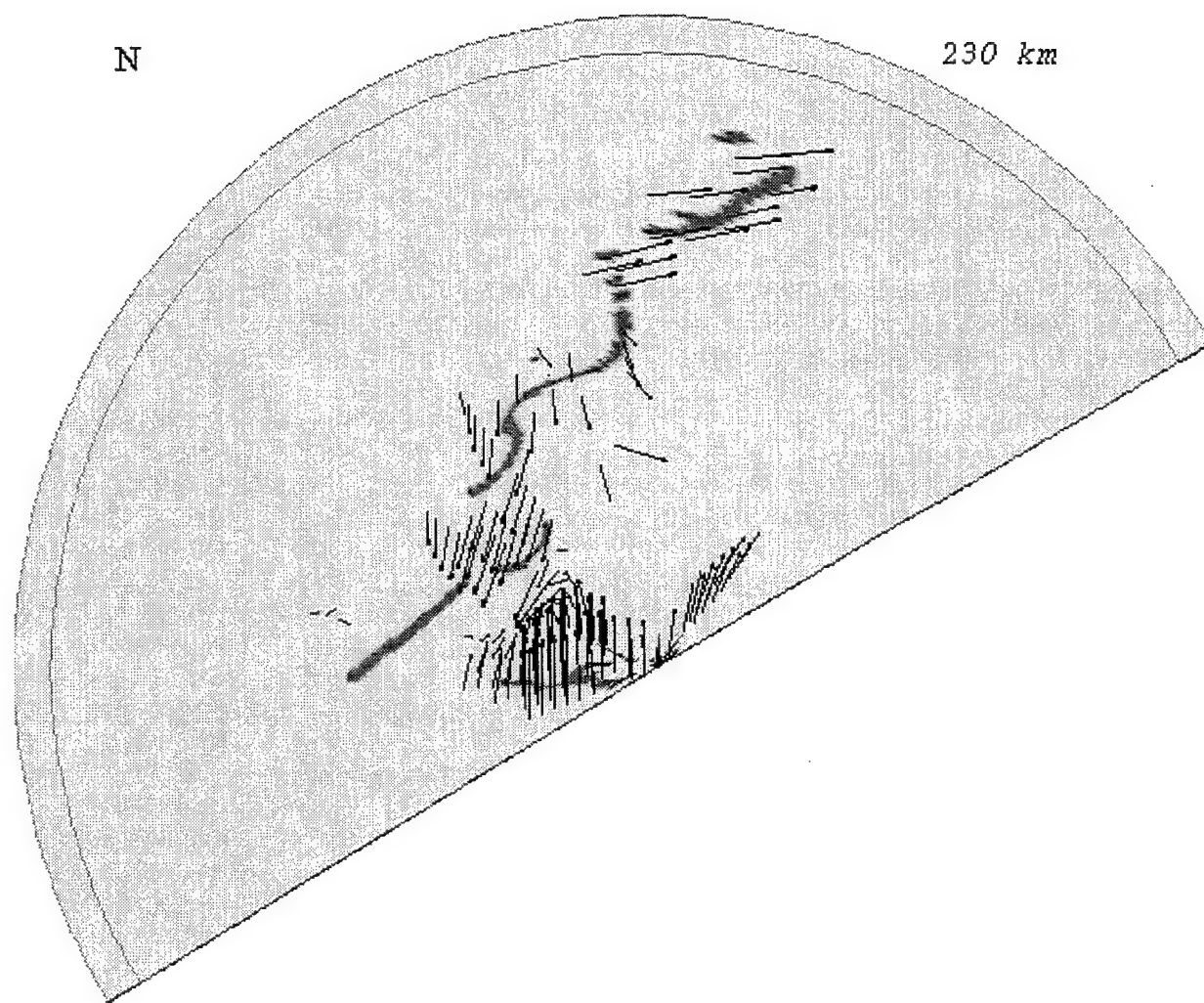


**Figure 9a** Wind behind and ahead of front at 0142.

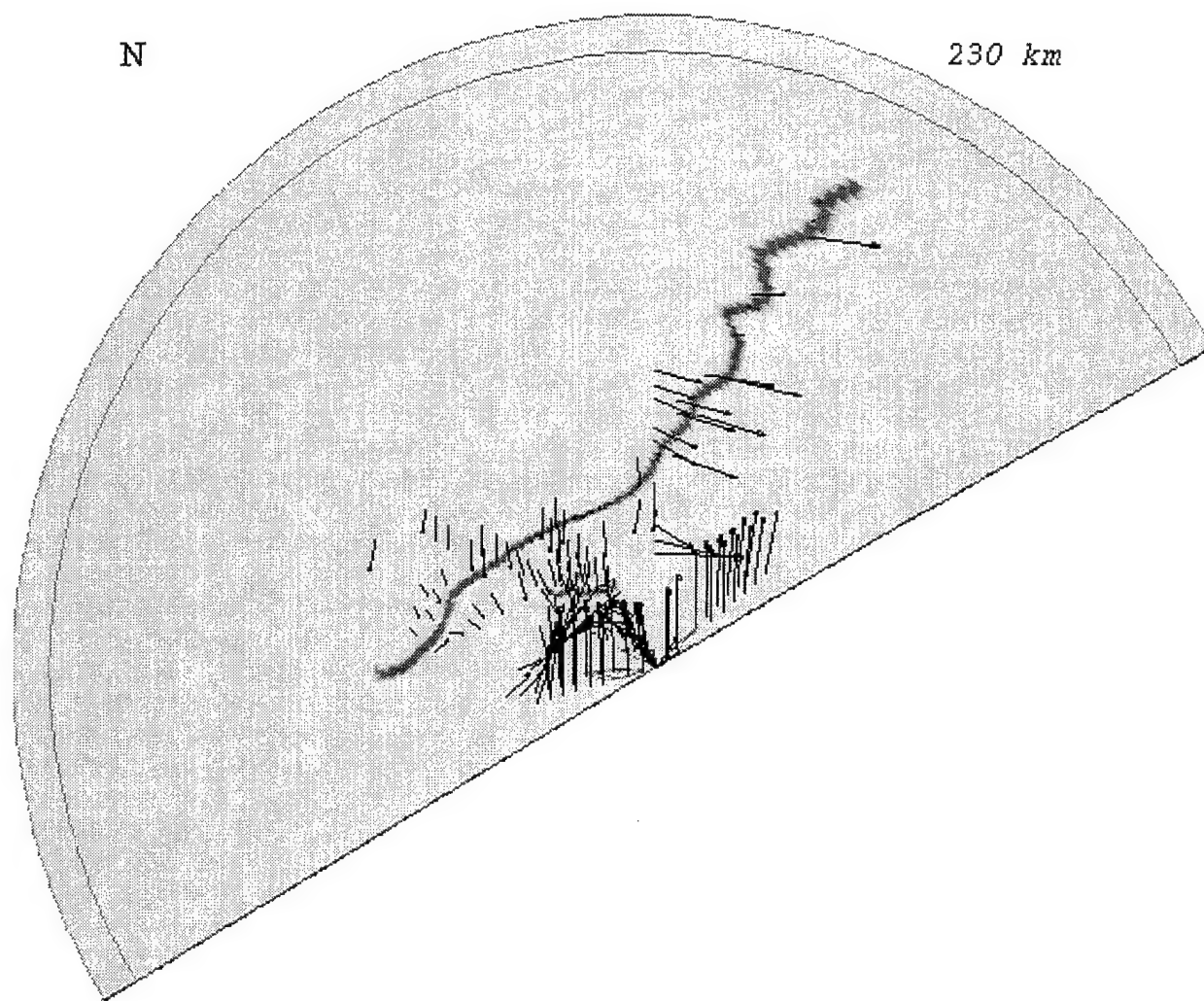


**Figure 9b** Wind behind and ahead of front at 0227.

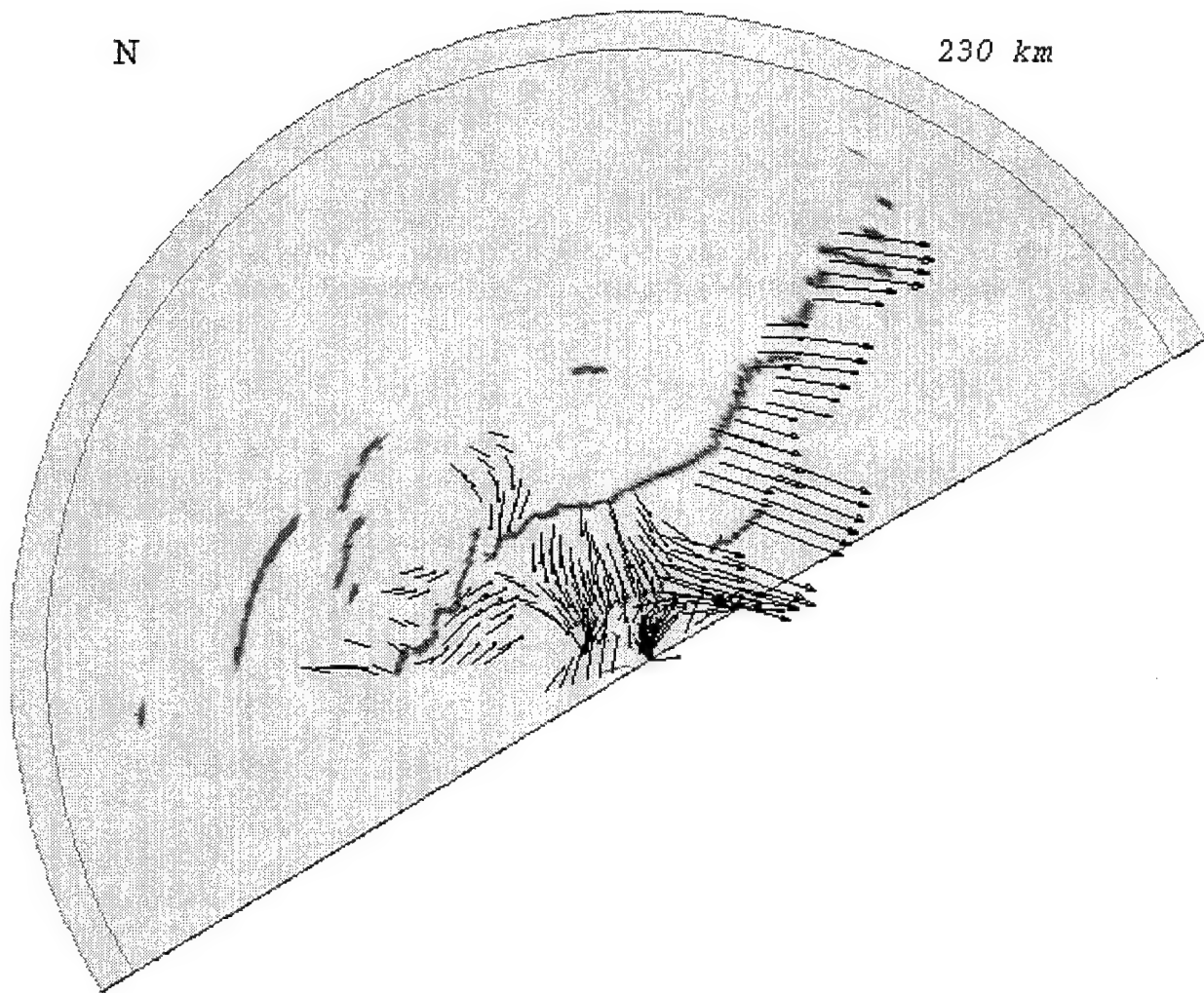


**Figure 9c** Wind behind and ahead of front at 0247.

## **5 TIME EVOLUTION**

### **5.1 *General Evolution***

#### **5.1.1 Initial period (2247 05/22/93 - 0142 05/23/93)**

During this time period, the cold front advances toward the radar from the northwest. The precipitation is predominately stratiform in nature (Figure 3a), with very little evidence of convection. With time, precipitation along the front slowly develops. Ahead of the front there is a thin line that is seen only in the lowest elevation scans. This line moves toward the front, consistent with the environmental flow.

#### **5.1.2 Rapid development period (0142 - 0342)**

The thin line seen earlier intersects with the cold front at the start of this period which appears to trigger a period of significant precipitation development and evolution. Following this collision, convection is sharply enhanced as evidenced by the stronger and more line-like reflectivity factor structure. Further, a gust front is observed to emanate from the front and to propagate toward the southeast, faster than, and hence away, from the front. The strongest convergence tends to be along the gust front and is confined to a very shallow layer. Convection associated with this convergence appears to be minimal as seen in the lack of significant precipitation development along the gust front. The convergence patterns associated with the front are much deeper and more consistent with the convective development that occurs.

#### **5.1.3 Convective dissipation period (0342 - 0523)**

With time, the gust front advects away from the cold front and appears to shut off the inflow to the cold front convection. The precipitation pattern along the front broadens and weakens, i.e., becomes much more stratiform in nature.

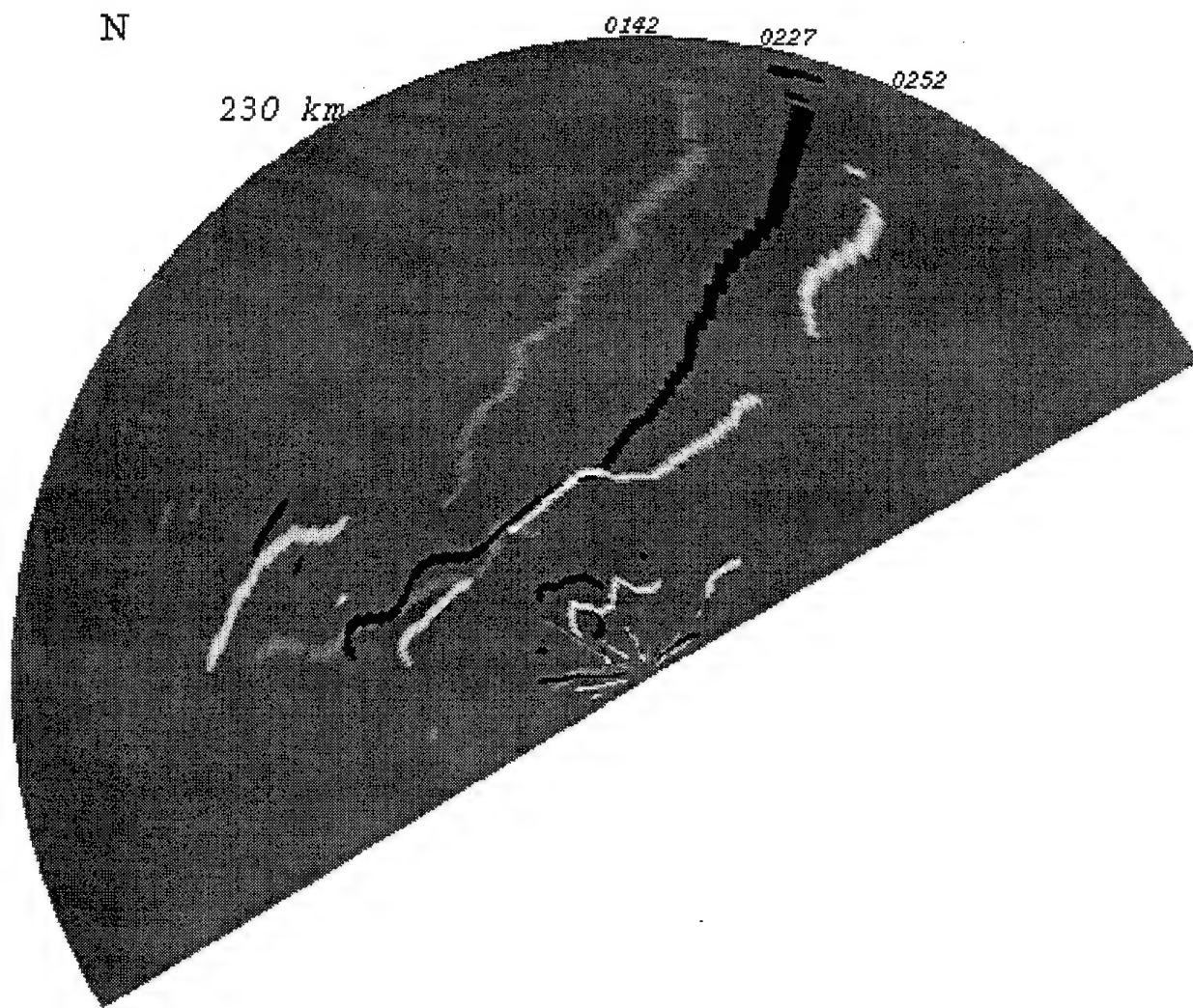


**Figure 10** Detected frontal lines at 0142, 0227, and 0252.

## 5.2 Front Characteristics

Figure 10 depicts the location of the detected frontal lines during the two-hour period from 0142 to 0342 and Table 1 summarizes some of the frontal characteristics. The front is detected over a length of at least 250 km throughout the period. The eastern portion of the frontal lines propagate about 16 m/s, while the western portion moves much more slowly. This motion is consistent with the wind estimates derived from the uniform wind sector analysis presented in Section 4. Because of this differential motion, the front swings from a more northerly orientation to a more easterly one. It appears, but has yet to be confirmed, that the uniform wind estimates may give estimates to frontal motions and orientations.

TABLE 1. Summary of Frontal Characteristics

		Initial Period	Rapid Development Period						Dissipation Period
Time		01:42	02:07	02:17	02:27	02:37	02:47	02:52	03:42
Motion (m/s)	East	16	16	16	16	16	16	16	16
	Middle	8	8	8	8	8	8	8	8
	West	0	0	0	0	0	0	0	0
	Gust	6	6	6	6	6	6	6	6
Length (km)		310	300	290	320	270	260	260	200
Angle		45°	15°	15°	30°	30°	45°	45°	60°
Slope		0.023	0.026	0.026	0.027	0.026	0.028	0.028	0.031

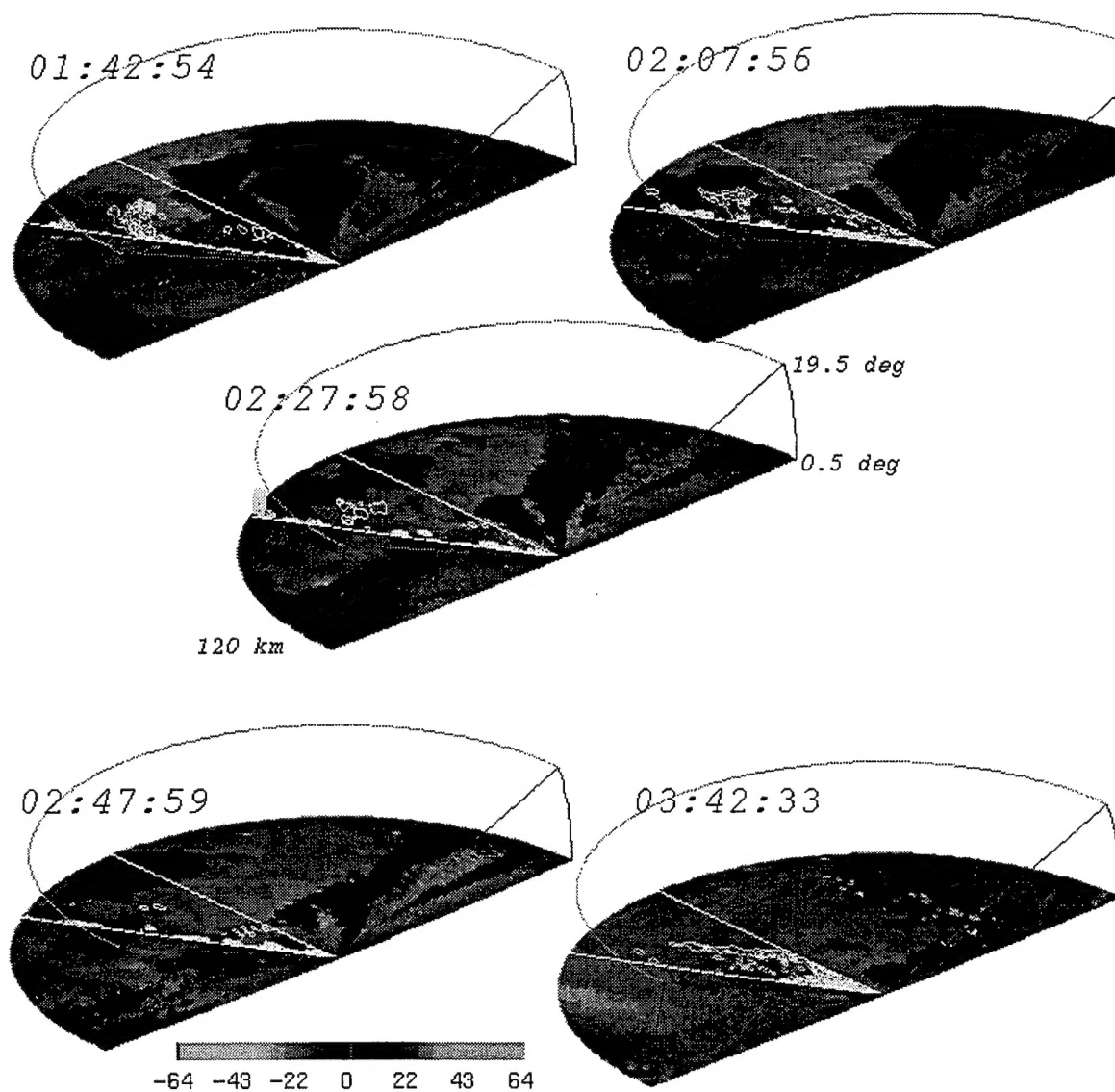


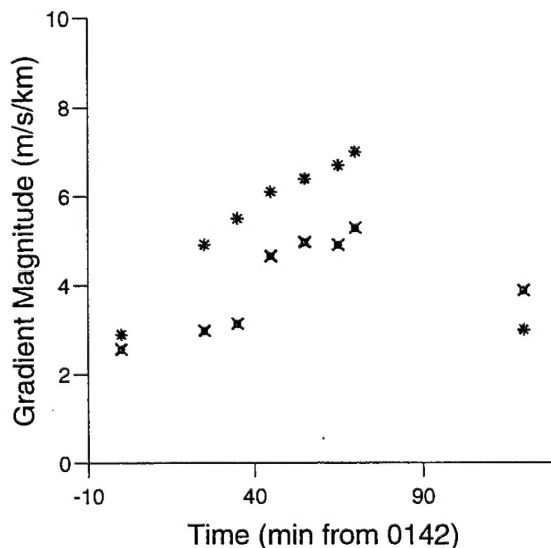
**Figure 11** Radial velocity gradient contours in vertical plants oriented along the 300° azimuth during the period 0142 to 0342.



### 5.3 Gradient intensity and convective strength

Figure 11 depicts the radial velocity gradient contours in vertical planes oriented along the 300° azimuth during the period 0142 to 0342. The strong convective regions are somehow relative to the gradient intensity. Along the southwest end of the front, the gradient maxima are initially vertically oriented through all heights; there are two distinct zones at the surface and the top of cold front boundary. With time, the surface maxima decouples from the cold front and moves ahead of the cold front. The whole time, intense convective development occurs at the top of the cold front.

Figure 12 depicts the trends for the means and maximums of radial velocity gradient magnitudes in the detected frontal region. “\*” indicates the mean gradient magnitude (scaled by a factor of 100) within the frontal zone and “x” indicate the maximum gradient magnitudes. The trends show that the gradients increase during the front development (0217 - 0252) and weaken rapidly while the convection is dissipating.





## 6 SUMMARY

An automatic frontal structure algorithm has been developed and applied to the Dodge City cold front case. The time evolution of the wind and precipitation has been analyzed based on the Doppler radar data. Results are encouraging. The cold front and an associated gust front are identified by using image processing techniques. The development of the front has been monitored through application of the gradient algorithm. Further refinement of the analysis techniques and application to more cases for verification purposes is required.

## 7 REFERENCES

- Harris, F.I., R.J. Donaldson, Jr., D.J. Smalley, and S-L Tung, 1994: Radar Studies of Aviation Hazards,.Phillips Laboratory, PL-TR-94-2146, 84 pp, ADA285845
- Hamann D.J., 1991: Extraction of fronts from Doppler radar images. Preprints, 25<sup>th</sup> Conf. on Radar Meteorol., AMS, Boston, MA, pp 119-122.
- Hermes, L.G., A. Witt, S.D. Smith, D.Klinge-Wilson, D. Morris, G.J. Stumpf, and M.D. Eilts, 1993: The gustfront detection and wind shift algorithms for the Terminal Doppler Weather Radar System. J. Atmos. Oceanic Technol., 10, 693-709.
- Tung, S-L, D.J. Smalley, F.I.Harris, and A.R. Bohne, 1995: Evolution of three-dimensional frontal structure. Preprints, 27<sup>th</sup> Conf. on Radar Meteorol., AMS, Boston, MA, pp 488-490.
- Wilson, J.W., and W.E. Schreiber, 1986: Initiation of convective storms at radar observed boundary layer convergence lines. Mon. Wea. Rev., 114, 2516-2536.